Wideband, Wide-Scan Planar Array of Connected Slots Loaded With Artificial Dielectric Superstrates

Syed, Waqas H.; Cavallo, Daniele; Thippur Shivamurthy, H.; Neto, A.

DOI
10.1109/TAP.2015.2507167

Publication date
2016

Document Version
Accepted author manuscript

Published in
IEEE Transactions on Antennas and Propagation

Wideband, Wide-Scan Planar Array of Connected Slots Loaded with Artificial Dielectric Superstrates

W. H. Syed, *Student Member, IEEE*, D. Cavallo, *Member, IEEE*, H. Thippur Shivamurthy, and A. Neto, *Senior Member, IEEE*

***Abstract*— Microwave broadband wide-scan antenna arrays are typically implemented resorting to vertical arrangements of printed circuit boards (PCBs). Here, we propose a planar solution realized with a single multi-layer PCB, with consequent reduction in cost and complexity of the array. It consists of an array of connected slots backed by a metallic reflector and loaded with superstrates. Artificial dielectric layers (ADLs) are used in place of real dielectrics to realize the superstrates, as they are characterized by very low surface-wave losses. For the unit-cell design we developed an analysis tool based on closed-form expressions and thus requiring minimal computational resources. Finite-array simulations are also performed by generalizing the analysis method to account for the truncation effects. The presence of the ADL superstrate allows reducing the distance between the array plane and the backing reflector while maintaining good matching performance. A realistic feed structure is also proposed, which consists of a microstrip line connected to a coaxial feed. Such a solution does not require balanced-to-unbalanced transitions, which often limit the achievable bandwidth. The proposed structure achieves in simulations more than an octave bandwidth (6.5 to 14.5 GHz), within a scanning range of $\pm 50^{\circ}$ in all azimuth planes.**

***Index Terms*— Artificial dielectric, connected arrays, wideband arrays, wide-scan array.**

I. Introduction

WIDEBAND, wide-scanning arrays have been receiving great attention in the last few decades for both commercial and military applications, such as satellite communications, radioastronomy and broadband radars.

The high number of coexisting systems that support various functionalities (e.g. tracking, surveillance or discrimination), for airborne military platform, has lead to an increasing interest in wideband arrays [1], [2]. In these scenarios, where space and weight are major constraints, it is beneficial to combine several functionalities in a single wideband, wide-scan antenna aperture. When such systems are required to support communication services, polarization purity is an important aspect to be accounted for. A dual-polarized wideband array with low cross-polarization was proposed in [3], for satellite communication applications. Another important application that benefits from wideband arrays is radio astronomy, e.g. the Square Kilometer Array (SKA) [4]–[7].

The most typical antenna solutions used in wideband, wide-scanning arrays can be mainly classified in three categories: stacked patches, tapered slot antennas, and connected arrays. Stacked patches have been shown to achieve about an octave bandwidth, for a linearly polarized array, capable to scan up to 45° in all azimuth planes [8]. However, the maximum possible bandwidth achievable with this solution is limited by the resonant nature of the radiators. Tapered slots have been shown to achieve large bandwidth of operation (multi-octave), over a wide scan volume [1], [9]. Despite the good performance in terms of impedance matching, the large bandwidth come often at the cost of degraded performance in terms of polarization purity, especially for scanning in the diagonal planes [10].

Connected arrays consist of arrays of either slots or dipoles which are electrically connected [11]. They have the advantage of being broadband and, at the same time, they can achieve low cross-polarization levels. Tapered slot antennas are intrinsically characterized by poor polarization performance because of the vertical components of the radiating currents along the flared edges. On the contrary, connected array are based on planar radiating currents with no vertical contribution, which can guarantee better polarization purity. Although this is true in principle, practically the feeding network of connected arrays must be carefully designed to maintain the undesired radiation from the feed lines as low as possible in all scanning conditions. Some examples of designs with low cross polarization levels were presented in [3], [12]–[14].

Unlike resonant antennas, which support sinusoidal and strongly frequency dependent current distributions, connected arrays are characterized by currents that are weakly frequency dependent, due to the electrical connection between adjacent antenna elements [15]. Practically the bandwidth of a connected array is limited by the presence of the backing reflector, which is needed to ensure unidirectional radiation [2].

In most of the state-of-the-art designs of dual-polarized Vivaldi and connected arrays [9], [13], [16], a complicate egg-crate configuration is implemented (see Fig. 1), which is costly to realize. In this assembly, vertical printed circuit boards (PCBs) are arranged in a three-dimensional lattice to provide unidirectional radiation. In Vivaldi arrays, a long vertical flaring is used in the element to increase the directivity. In connected arrays, a backing reflector is typically placed at about a quarter wavelength distance from the array plane [17], thus vertical feeding lines are needed to connect the elements

Manuscript received Month DD, YYYY; revised Month DD YYYY. First published Month DD, YYYY; current version published Month DD, YYYY. This work was supported by the European Research Council starting grant ERC-2011-StG AAATSI no. 278794, by the Dutch technology foundation (STW) under project code 10709, and by the Netherlands Organization for Scientific Research (NWO) VENI Grant no. 13673.

The authors are with the Microelectronics Department of the EEMCS Faculty, Delft University of Technology, 2628 CD Delft, The Netherlands (e-mail: w.h.syed, d.cavallo, a.neto@tudelft.nl).

Color versions of one or more of the figures in this paper are available online at http://ieeexplore.ieee.org.

Digital Object Identifier XX.XXXX/TAP.XXXX.XXXXXXXX.

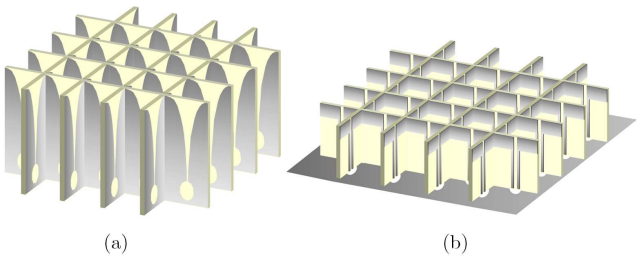

Fig. 1. Typical egg-crate configuration for wideband wide-scanning dual-polarized arrays: (a) tapered slot antenna array and (b) connected dipole array.

to the connectors or electronic components located below the ground plane. These lines are usually too long, e.g. for X- or Ku-band designs, to be implemented with standard PCB via-hole technology and thus they are printed on vertically oriented PCBs.

To overcome the drawbacks of the vertical arrangement of the antenna PCBs, it is convenient to implement the array in a completely planar structure that, as such, would be low-cost and easier to manufacture. A planar solution for wideband phased array was presented in [14], where scanning up to $45°$ degrees was achieved, with active voltage standing wave ratio (VSWR) lower than 2.8. Here we propose a different concept that allows to further increase the scanning range to $50°$, while maintaining good matching efficiency (VSWR$<$ 2) within a large frequency bandwidth.

A. Antenna Concept

In the proposed solution, we combine the connected array with artificial dielectric layers (ADLs). A connected array of slots in presence of a backing reflector is depicted in Fig. 2(a), with the respective geometrical parameters. Connected slots are selected as radiating elements, to avoid the use of differential feed lines, which can support undesired common-mode resonances [7]. Indeed, the slot elements can be fed by unbalanced lines, as opposed to dipole elements, which often require differential feeding lines and ad-hoc balanced-to-unbalanced (baluns) transitions [12], [18]. Such baluns are often the limiting factor for the bandwidth performance.

Figure 2(b) shows a unit cell of the connected array loaded with an ADL superstrate, located at a distance h_{gap}. ADLs consist of arrays of electrically small metallic patches included in a dielectric host medium to enhance its equivalent relative permittivity, as shown in Fig. 3. The factor by which the permittivity of a medium is increased depends on the physical dimensions of the metallic patches and the inter-layer distance [19], [20]. ADLs have been recently used to enhance the front-to-back ratio of planar antennas and to minimize the excitation of the surface waves [21].

Therefore, when loaded with a single or multiple ADL slabs, the array 'feels' less the presence of the backing reflector, which can be located closer to it without strongly degrading the impedance matching properties. This reduced distance between the array and the backing reflector allows the implementation of the element feed by means of standard via-hole technology, e.g. for X- or Ku-band designs. Consequently,

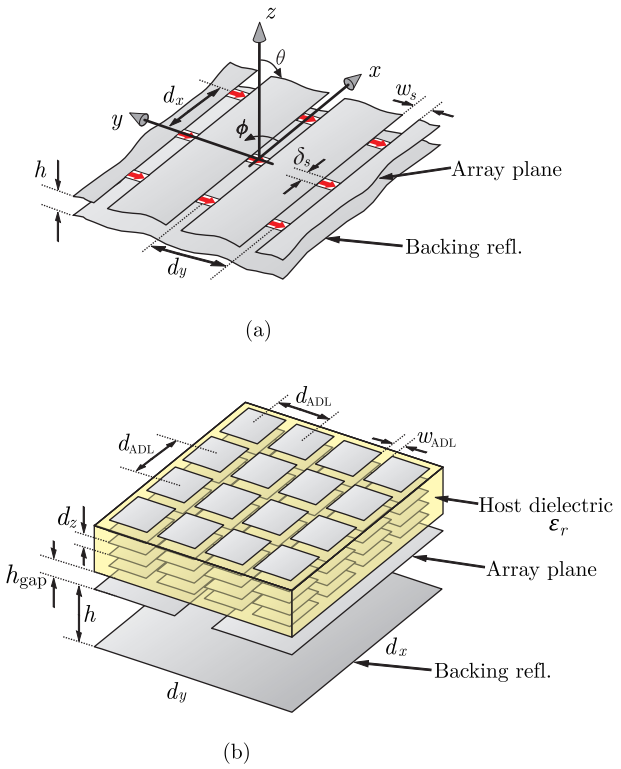

Fig. 2. (a) Connected array of slots in the presence of a backing reflector and (b) unit cell of the array loaded with ADL.

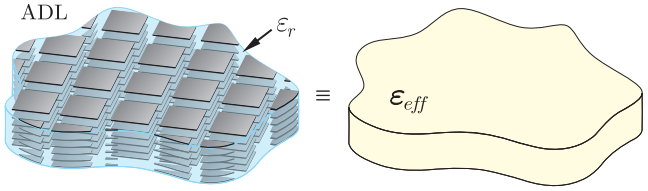

Fig. 3. A planar ADL slab hosted by a homogeneous dielectric of permittivity ε_r to realize an equivalent anisotropic medium.

a fully planar implementation of the array is enabled by the proposed solution. The ADL slab is characterized by a high effective relative permittivity, thus increasing the radiation towards the positive z-direction.

The analysis of the array concept presented here is based on infinite array simulations. Several design examples are shown in the paper, for single-polarized arrays targeting the frequency range of one octave, from 6.5 to 14.5 GHz, and scanning up to $50°$ in all azimuth planes. A possible implementation of the feed structure and the multi-layer stack is also investigated.

II. Analysis Tool

Simulating a unit cell like the one in Fig. 2(b) using commercial electromagnetic solvers is not a simple or fast process, due to the large number of layers composing the entire stack and the electrically small geometrical features that require very fine meshes. Finite array simulations are even more demanding in terms of computational resources and could become prohibitive for a large number of layers.

Moreover, a high number of such simulations are needed for the optimization of the total structure, rendering the design impractical. For these reasons, we developed a spectral method to estimate the performance of the connected array of slots loaded with ADL. The formulation exploits and combines the analytical spectral solutions of connected arrays [17] and ADLs [19], [20]. The analysis tool takes into account all the higher-order-mode interactions between adjacent layers composing the array plane and the ADL. This is required since the inter-layer distance is typically in the order of one hundredth of the wavelength. The method is used to predict the active impedance of the array unit cell, but it is also generalized to estimate the finite array performance.

A. Infinite Periodic Array

The active input impedance of the connected array of slots can be expressed as follows [17]:

$$z_{\text{act}} = -\frac{1}{d_x}\sum_{m_x=-\infty}^{\infty}\frac{\text{sinc}^2(k_{xm}\frac{\delta_s}{2})}{D(k_{xm})}. \tag{1}$$

This consists in an infinite summation of Floquet modes (with indexes m_x and wave numbers $k_{xm} = k_{x0} - 2\pi m_x/d_x$, accounting for the periodicity along the x-axis. Here, $k_{x0} = k_0 \text{sin}\theta\text{cos}\phi$, where k_0 is the propagation constant in the free space and θ, ϕ are the angles towards which the array is pointing. The function $D(k_x)$ represents the transverse connected array Green's function [17] and accounts for the periodicity along the y-axis and for the stratification along z. It is expressed as a summation of Floquet modes with wave numbers $k_{ym} = k_{y0} - 2\pi m_y/d_y$ and $k_{y0} = k_0 \text{sin}\theta\text{sin}\phi$:

$$D(k_x) = \frac{1}{d_y}\sum_{m_y=-\infty}^{\infty} G_{xx}(k_x, k_{ym}) J_0\left(k_{ym}\frac{w_s}{2}\right). \tag{2}$$

The zeroth order Bessel function (J_0) is the Fourier transform of the transverse edge-singular magnetic current distribution along the slot. Moreover, G_{xx} is the spectral Green's function that represents the x-component of the magnetic field radiated by a x-oriented elementary magnetic dipole. This Green's function accounts for the stratification along the z-axis and it can be defined to include the ADL slabs. It can be conveniently expressed in terms of the current solutions of equivalent transmission lines that represent the layered media above and below the plane of the slots [22]:

$$G_{xx}(k_x, k_y) = G_{xx,\text{up}}(k_x, k_y) + G_{xx,\text{down}}(k_x, k_y) = \\ -\frac{I_{\text{up,TE}}k_x^2 + I_{\text{up,TM}}k_y^2}{k_\rho^2} - \frac{I_{\text{down,TE}}k_x^2 + I_{\text{down,TM}}k_y^2}{k_\rho^2} \tag{3}$$

where $k_\rho^2 = k_x^2 + k_y^2$. The currents at the plane $z = 0$ are given by

$$I_{\text{up},Ti} = \frac{1}{Z_{\text{up},Ti}}; \quad I_{\text{down},Ti} = \frac{1}{Z_{\text{down},Ti}} \tag{4}$$

where Ti can refer to either the transverse electric (TE) or the transverse magnetic (TM) mode. The impedances representing the upper and lower stratifications are calculated using the equivalent circuit models in Fig. 4. In these models,

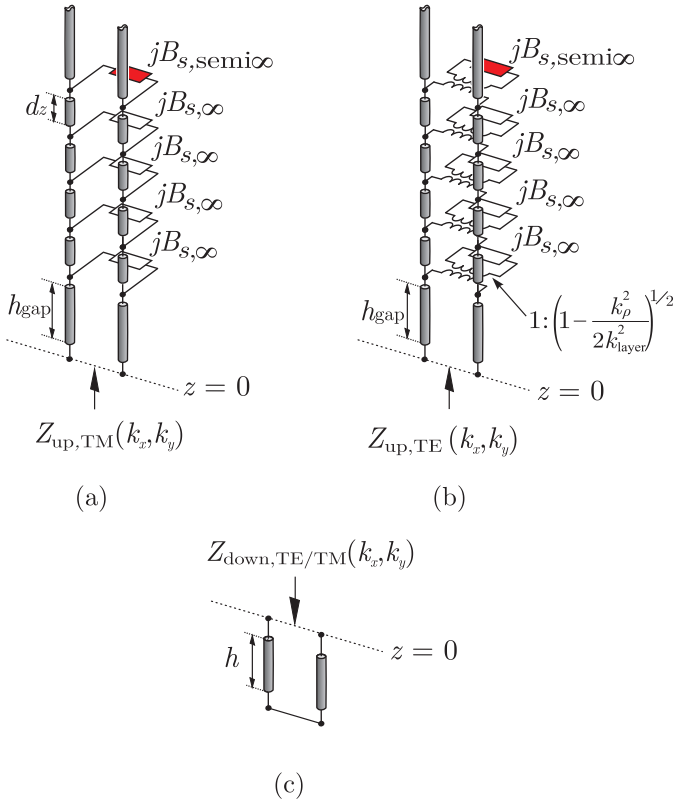

Fig. 4. Equivalent transmission-line model of a finite-height ADL for a generic (a) TM and (b) TE plane wave; (c) equivalent shorted line representing the backing reflector.

the transmission lines for the TE and the TM incidence have characteristic impedances $Z_{0\text{TE}} = \zeta k/k_z$ and $Z_{0\text{TM}} = \zeta k_z/k$, respectively, with ζ and k being the impedance and the wavenumber of the pertaining dielectric slab and with $k_z = (k^2 - k_{x0}^2 - k_{y0}^2)^{1/2}$. Each layer of the ADL is represented as an equivalent susceptance ($B_{s,\infty}$) defined in closed form in [20]. The finite height of the ADL is taken into account using a semi-infinite solution for the top layer, represented as $B_{s,\text{semi}\infty}$ [20]. The transformer with turn ratio $1 - k_{\rho m}^2/(2k_{\text{layer}}^2)$ in the TE equivalent circuit in Fig. 4(b) was derived in [20]. $k_{\rho m}^2$ can be written in terms of the incident angle for homogeneous plane waves (visible region) or, more in general, we consider $k_{\rho m}^2 = k_{xm}^2 + k_{ym}^2$ to treat also the cases of non-homogeneous plane waves (higher order Floquet modes). In the expression of the transformer, k_{layer} represents the propagation constant of the medium in which the layer (array of patches) is embedded or it is an average propagation constant if the layer is located at the interface between two different media.

It can be noted that the TE and TM equivalent transmission lines of the ADL slab, shown in Fig. 4, are decoupled. This is not valid in general, but it is a low-frequency approximation. A more general equivalent circuit, which includes the coupling circuit between TE and TM in analytical form, was given in [19], [20]. There it was demonstrated that it is possible to neglect the coupling effects under the assumption that the ADLs are composed by electrically small patches ($< \lambda/4$).

By implementing the equations (1) to (4) in a Matlab code,

TABLE I

DIMENSIONS OF THE ARRAY UNIT CELL IN FIG. 2(b); λ_0 IS THE FREE-SPACE WAVELENGTH AT THE MAXIMUM FREQUENCY OF INVESTIGATION f_0

$d_x = d_y$	w_s	δ_s	h	h_{gap}	d_{ADL}	w_{ADL}	d_z
$\frac{\lambda_0}{2.15}$	$\frac{\lambda_0}{47.5}$	$\frac{\lambda_0}{11.1}$	$\frac{\lambda_0}{12.5}$	$\frac{\lambda_0}{78.7}$	$\frac{\lambda_0}{10.7}$	$\frac{\lambda_0}{111}$	$\frac{\lambda_0}{157.3}$

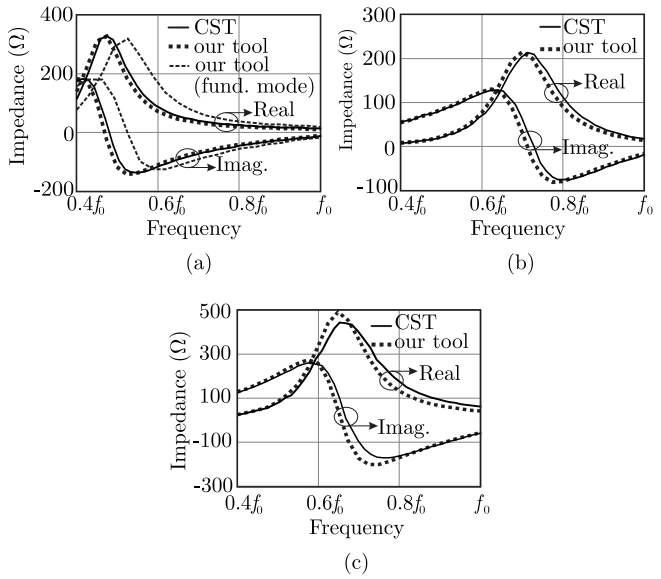

Fig. 5. Comparison of the input impedance of the connected array of slots loaded with ADL for (a) broadside, scanning to 50° in the (b) E- plane and in the (c) H-plane.

we obtain an analytical tool to estimate the matching performance of the array unit cell. As an example, a comparison between our tool and the commercial electromagnetic solver CST [23] is presented in Fig. 5. The figure reports the active input impedance of an ADL-loaded array with the geometrical dimensions summarized in Tab. I. A total of 5 layers are used in the ADL design, realizing an effective dielectric constant of 8.4 for normal incidence. The dielectric of the host medium is taken to be free space $\varepsilon_r = 1$. A good comparison is obtained for broadside and scanning towards 50° in the E- and H-planes, as shown in Fig. 5. The calculation of the active input impedance, for 15 frequency points and 3 scan angles, can be completed in 0.2 seconds with our code, while it requires about 63 minutes with CST, on the same computer.

The method described in [19], [20] is, to our knowledge, the only analytical model accounting for the higher-order interaction between the multiple layers composing the ADL. To highlight the importance of taking into account the higher-order coupling, Fig. 5(a) also reports the result obtained by considering only the interaction of the propagating Floquet mode (above cutoff). The result does not agree anymore with the CST full-wave simulations, showing a 10% shift of the resonance peak.

B. Finite × Infinite Array

The model of the connected array loaded with ADLs, presented in the previous subsection, is based on the infinite array approximation. However, it is known that finiteness effects can be significant, especially for wideband arrays that are characterized by high mutual coupling [24]. For this reason, it is of interest to generalize the expression of the active input impedance in (1) to account for the finite number of elements. By assuming the array to be infinitely periodic along the y-direction and finite along x (see Fig. 6(a)), the active input impedance of the n_x-th element can be expressed as

$$z_{\text{act},n_x} = (i_{n_x}/v_{n_x} - 1/Z_l)^{-1} \tag{5}$$

where i_{n_x} and v_{n_x} represent the current and the voltage at the n_x-th port (feed), whereas Z_l is the source impedance at the ports. The voltages across the terminals of all the N_x feeds can be related to the excitation currents following the same procedure described in [24], [25]

$$\mathbf{v} = \left[\frac{1}{Z_l}\mathbf{Z} + \mathbf{I}\right]^{-1} \mathbf{Z} \cdot \mathbf{i} \tag{6}$$

where $\mathbf{I}$ is the identity matrix and $\mathbf{Z}$ is a square matrix composed by the mutual impedances between any pair of elements of the array (n_x, n'_x):

$$z_{n_x n'_x} = -\frac{1}{2\pi} \int_{-\infty}^{\infty} \frac{\text{sinc}^2(k_x \frac{\delta_s}{2}) e^{-jk_x(n_x - n'_x)d_x}}{D(k_x)} dk_x \,. \tag{7}$$

In (6), $\mathbf{i}$ is the vector of the excitation amplitudes of the elements. This complex weights account for the phase shift of the elements when the array is scanned and for possible amplitude tapers of the array excitation. The integral in (7) can be calculated numerically with an appropriate deformation of the integration path in the complex k_x-plane to ensure fast convergence, as it was done in [24].

The finiteness along the direction orthogonal to the slots (E-plane) can also be taken into account. If the array is composed

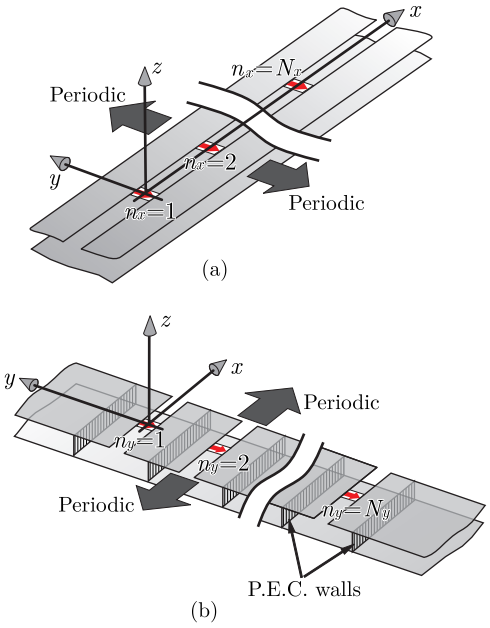

Fig. 6. (a) Finite × infinite array of connected slots: (a) finiteness along x (H-plane) and (b) along y (E-plane).

by $\infty \times N_y$ elements, the active input impedance of the n_y-th element is given by [25]

$$z_{\text{act},n_y} = -\frac{1}{d_x} \sum_{m_x=-\infty}^{\infty} \frac{\text{sinc}^2(k_{xm}\frac{\delta_s}{2})}{D_{n_y}(k_{xm})} \tag{8}$$

where

$$D_{n_y}(k_{xm}) = \frac{1}{2\pi} \sum_{n'_y=1}^{N_y} \frac{i_{n'_y}}{i_{n_y}} \cdot \int_{-\infty}^{\infty} G_{xx}(k_{xm}, k_y) J_0\left(k_y \frac{w_s}{2}\right) e^{-jk_y(n_y-n'_y)d_y} dk_y \,. \tag{9}$$

The integral in (9) is poorly convergent, due to pole singularities of the Green's function term $G_{xx,\text{down}}$ in (3). These poles are associated with parallel plate waveguide (PPW) modes propagating between the array plane and the backing reflector. Such modes are excited at the edge of the array when finiteness on the E-plane is introduced and they propagate with low attenuation along the entire array, thus affecting the active impedance of all the elements. To improve the convergence of the solution, we consider a slightly different geometry where vertical walls, modeled as perfect electric conductor (PEC), are inserted between parallel slots, as shown in Fig. 6(b). These walls can be practically implemented with vias and will be shown in Sec. IV to effectively overcome unwanted resonances caused by the feeding structure. To include the PEC walls in the formulation, it is convenient to modify (9) to explicitly express the two terms of the Green's function relative to the stratification above and below the plane of the slots:

$$D_{n_y}(k_{xm}) = D_{n_y,\text{up}}(k_{xm}) + D_{n_y,\text{down}}(k_{xm}) \,. \tag{10}$$

The first term can be calculated as

$$D_{n_y,\text{up}}(k_{xm}) = \frac{1}{2\pi} \sum_{n'_y=1}^{N_y} \frac{a_{n'_y}}{a_{n_y}} \cdot \int_{-\infty}^{\infty} G_{xx,\text{up}}(k_{xm}, k_y) J_0\left(k_y \frac{w_s}{2}\right) e^{-jk_y(n_y-n'_y)d_y} dk_y \tag{11}$$

where the integral does no longer exhibit the singularities due to the presence of the backing reflector and can be performed numerically. Moreover, due to the presence of the walls, the structure below the slot can be described by a periodic solution:

$$D_{n_y,\text{down}}(k_{xm}) = \frac{1}{d_y} \sum_{m_y=-\infty}^{\infty} G_{xx,\text{down}}\left(k_{xm}, \tfrac{-2\pi m_y}{d_y}\right) J_0\left(\tfrac{-2\pi m_y}{d_y}\tfrac{w_s}{2}\right) \,. \tag{12}$$

To validate the expressions in (5), (8) and (10)−(12), we report in Fig. 7 the active input impedance for a $9 \times \infty$ and a $\infty \times 9$ array. The dimensions of the array and the ADL slab are the same as specified in Tab. I. The impedance is shown as a function of the element index at the frequency $0.5 f_0$, when the elements are excited with uniform amplitudes and broadside scanning is assumed. The solution obtained with our spectral method is in fair agreement with CST finite-by-infinite simulations. It can be observed that the finite array results oscillate around the infinite array solution, and the oscillations are stronger at the edges of the array.

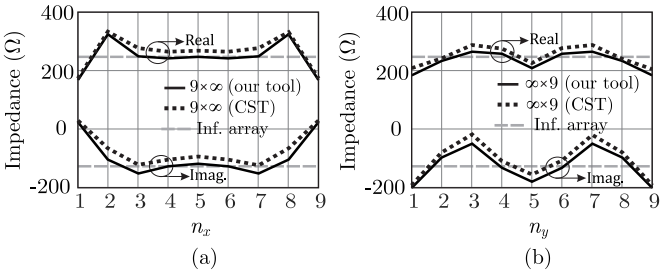

Fig. 7. Active input impedance for an array of (a) $9\times\infty$ and (b) $\infty \times 9$ elements, at the frequency $0.5 f_0$ and as a function of the element index. The unit-cell geometry is defined in Tab. I.

TABLE II
DIMENSIONS OF THE THREE ADL SLABS

Parameter	Unit	Slab1	Slab2	Slab3
d_{ADL}	(mm)	1.862	1.862	1.862
w_{ADL}	(mm)	0.19	0.2	0.4
h_{gap}	(mm)	0.45	0.5	0.33
d_z	(mm)	0.127	0.333	2
n_z	–	5	6	3
$\varepsilon_{r\text{eff}}$	–	16.5	5.5	1.72
ε_r	–	2.2	1	1

It should be noted that the choice of 9-element arrays loaded with a single ADL slab was made for the sake of validation of the introduced method and to maintain CST simulations manageable with our available computational resources. However, our model can be used to simulate much larger arrays with an arbitrary number of ADLs.

III. SINGLE-POL ARRAY DESIGN

In this section, we present the design of a single-polarized connected array of slots matched over an octave bandwidth in the target frequency range from 7 to 14 GHz. To realize a broadband transformation between the free-space impedance (377 Ω) and the slot active input impedance (70 Ω), three ADL slabs are considered. Figure 8(a) depicts the unit-cell of connected slot array loaded with the multi-slab ADL stack.

To enable the possibility of implementing a feeding structure with PCB via-hole technology, we consider a dielectric slab (RO5880LZ) of permittivity $\varepsilon_{r5880\text{LZ}} = 1.96$ between the slot plane and the backing reflector. When compared with a foam substrate, such a slab degrades the matching performance of the array. Therefore, to reduce its effective permittivity, the dielectric can be milled in a grid configuration as shown in Fig. 8(b). The equivalent dielectric constant, calculated as in [26], is reduced to 1.4 and it remains almost independent of the angle of the incidence of the plane wave. Also, a substrate of relative permittivity ε_{r5880} =2.2 and thickness 0.254 mm is included for the possibility of realizing a microstrip feed line (see Fig. 8(b)).

The analytical tool has been used to optimize the geometrical parameters of the ADL slabs and the connected

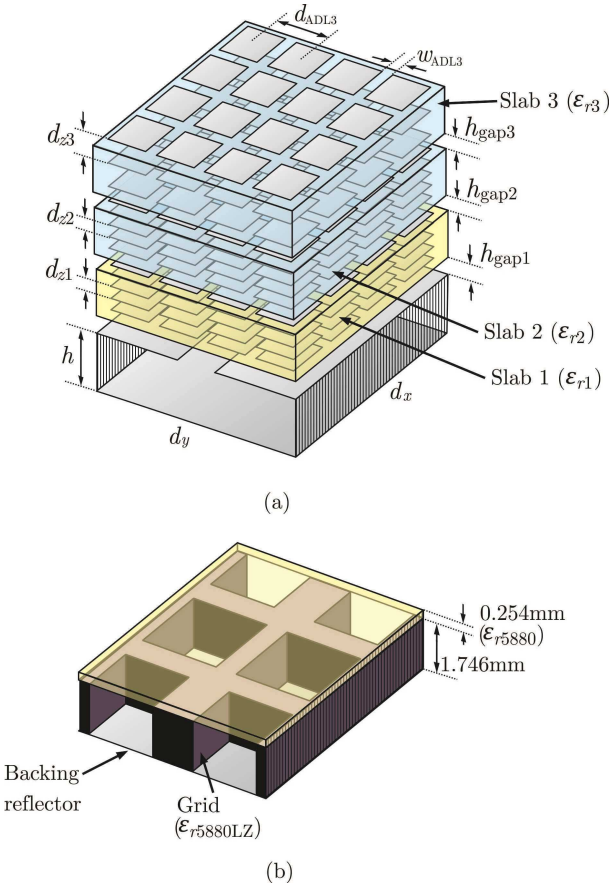

Fig. 8. (a) A unit cell of connected array radiating in the presence of multi-layer ADL stack; (b) exploded view of the dielectric stratification on the back side of the antenna.

TABLE III
DIMENSIONS IN mm OF THE SINGLE-POL CONNECTED ARRAY

$d_x = d_y$	w_s	δ_s	h
9.31	0.7	3.5	1.8

array, which are summarized in Tabs. II and III). The grid is modeled in our analytical tool as a homogeneous dielectric of permittivity 1.4 and height of 1.746 mm. The three ADL slabs are characterized by a number of layers (n_z) of 5, 6 and 3, respectively, and relative permittivity, for normal plane-wave incidence, of 16.5, 5.5, and 1.72, respectively. These three different dielectric constants can be engineered by varying the geometrical parameters of the ADL [19], [20]. It can be noted that the dimensions of the patches in the ADL slabs are less than one tenth of the wavelength i.e., $0.1\lambda_0$. Here, λ_0 is the wavelength in free space at the maximum frequency of investigation 14 GHz. Such a small size yields very low ohmic losses, in virtue of the non-resonant nature of the metal patches [27]. Moreover, under the hypothesis of small periods, the analytical tool developed in [19], [20] remains valid with high accuracy.

A. Matching Performance for Ideal Design

In Fig. 9, the active voltage standing wave ratio (VSWR) of the array normalized to 70 Ω is shown. The VSWR is lower

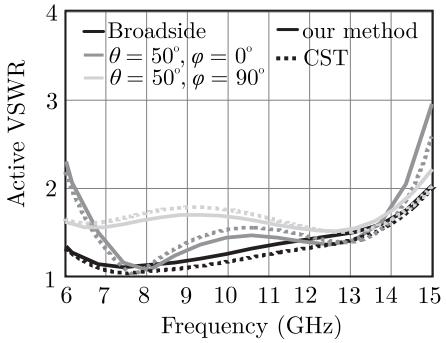

Fig. 9. Active VSWR of the array for broadside, scanning at 50° in E- and H-plane.

than 2 for over more than one octave bandwidth, for broadside and for scanning to 50° in the E- and the H-planes. These results assume that the array elements are fed with ideal delta-gap excitations, as shown in Fig. 2. A good agreement can be observed between the curves obtained with the presented analytical tool and the results obtained using a commercial electromagnetic solver [23].

Note that the distance from the backing reflector is remarkably low ($0.09\lambda_0$). This height is much lower than the typical value of $\approx \lambda_0/4$ required to maximize the bandwidth for slots with a backing reflector and without superstrates.

B. Surface Waves and Scan Blindness

One of the main advantages of the ADL superstrates compared to real dielectrics is the reduced loss due to surface waves. Typically, superstrates with high permittivity increase the front-to-back ratio of the array at the expenses of reduced scan range. This is not the case for the ADL loaded slabs [20].To clarify this aspect, Fig. 10 shows the dispersion curves of a grounded slab composed by the ADL superstrates defined in Tab. II. We compare these results with homogenous dielectric slabs with the same permittivity that the ADL synthesizes for broadside scanning. It is apparent that the surface waves supported by the real dielectric are characterized by much higher propagation constant, and consequently scan blindness occurs at smaller angles. The blind angle of a periodic array (with period d) of elementary magnetic dipoles located on a grounded slab can be easily calculated as

$$\theta_{sb} = \sin^{-1}\left(\frac{\lambda_0}{d} - \frac{k_{SW}}{k_0}\right). \tag{13}$$

For instance, if one assumes the frequency to be 15 GHz and the period to be 9.25 mm, scan blindness would occur at 34° for the case of homogeneous dielectric. On the contrary, no scan blindness would be observed for the ADL, as the argument of the $\sin^{-1}$ in (13) is greater than 1.

C. Inclusion of Bonding Layers

The practical realization of the multi-layer PCB composing the antenna array requires the use of bonding layers. A possible implementation of the layer stack is depicted in Fig. 11. The first ADL slab is realized using multiple Rogers

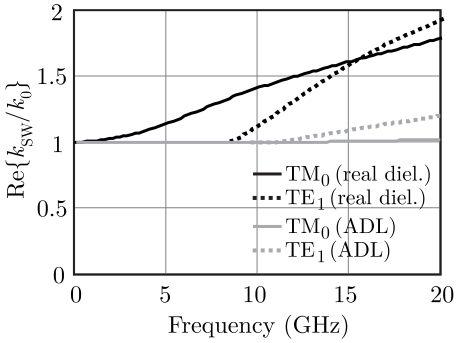

Fig. 10. Surface waves supported by grounded slabs composed of ADLs and equivalent homogenous dielectrics.

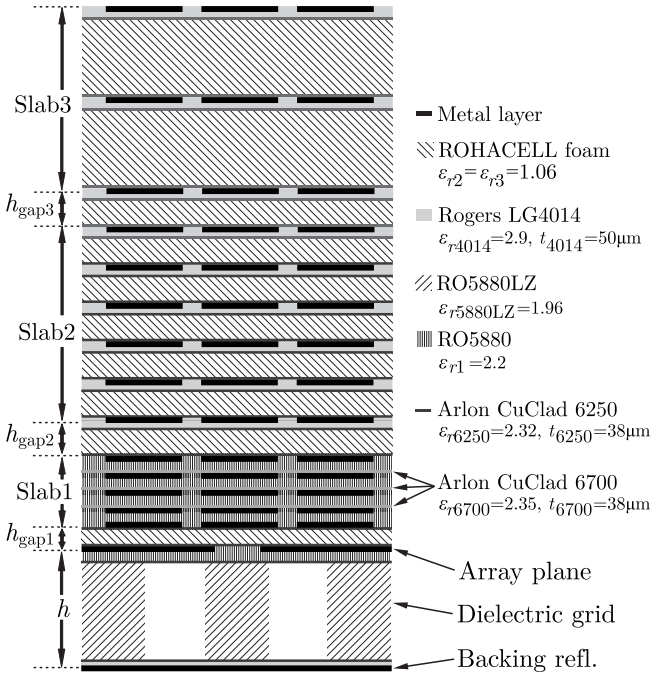

Fig. 11. A two dimensional view of the stratification with the inclusion of the bonding layers.

RO5880 substrates ($\varepsilon_{r1} = 2.2$, thickness $t_1 = 0.127$ mm), in order to achieve very small inter-layer spacing, which would be too demanding for foam substrates. Arlon CuClad 6700 ($\varepsilon_{r6700} = 2.35$, $t_{6700} = 0.038$ mm) is used to bond the slabs together. Rohacell foam ($\varepsilon_{r2} = \varepsilon_{r3} = 1.06$) can be used to realize the other two ADL slabs, for which the inter-layer distance is greater than 330 μm. Since foam cannot be metalized, the metal patches can be printed on a thin dielectric film (LG4014, $\varepsilon_{r4014} = 2.9$, $t_{4014} = 0.050$ mm) and this layer is glued to the foam using adhesive Arlon CuClad 6250 ($\varepsilon_{r6250} = 2.32$, $t_{6250} = 0.038$ mm), as done in [28].

The effect of the bonding layers onto the array performance is investigated in Fig. 12(a), which shows the active VSWR of the array with the inclusions of the glue. It can be observed that the presence of the bonds strongly degrades the matching efficiency of the array. For the specific targeted frequency range, the thickness of the adhesive layers is not negligible with respect to the total height, which increases by about 15%

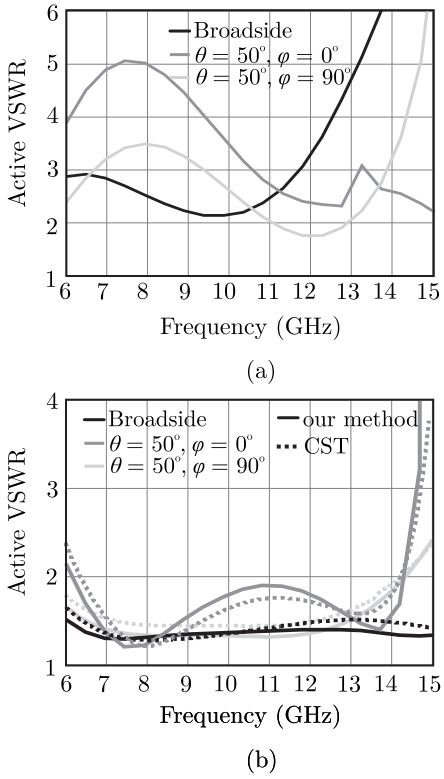

Fig. 12. (a) Deteriorating effect of the bonds on the active VSWR of Fig. 9; (b) re-optimized VSWR, accounting the effect of the bonds.

TABLE IV
ADL DIMENSIONS AFTER THE INCLUSION OF ADHESIVE FILMS.

Parameter	Unit	Slab1	Slab2	Slab3
d_{ADL}	(mm)	1.862	1.862	1.862
w_{ADL}	(mm)	0.19	0.2	0.4
h_{gap}	(mm)	0.424	0.474	2.1
d_z	(mm)	0.127	0.374	1.47
n_z	–	3	5	2
ε_r	–	2.2	1	1

TABLE V
DIMENSIONS IN mm OF THE SINGLE-POL CONNECTED ARRAY

$d_x = d_y$	w_s	δ_s	h
9.25	3.8	1.8	2.0

(from 7.1 to 8.1 mm). Smaller impact of the glue is expected for lower frequency designs.

However, this effect can be accounted for in the analytical model of the entire structure, which can be re-optimized including the presence of the adhesive layers. The optimization process resulted in a new set of geometrical parameters of the array and the ADL, which leads to performance similar to the case without bonding. The active VSWR of the array is reported in Fig. 12(b), reporting an active VSWR$<$2 from 6.3 to 14 GHz. CST simulations are also included in the figure for comparison. The optimized dimensions of the ADL and the connected array are listed in Tab. IV and V, respectively.

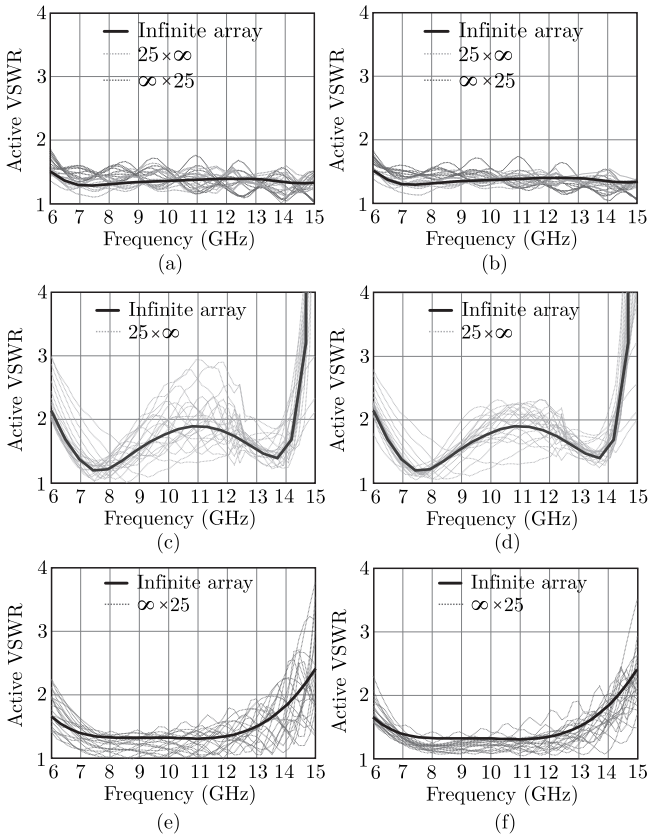

Fig. 13. Active VSWR of an array with $25 \times \infty$ and $\infty \times 25$ elements: (a), (c), (e) are relative to broadside, H-plane scan to 50° and E-plane scan to 50°, respectively, for uniform array illumination; (b), (d) and (f) refer to the same scanning conditions, but for a raised-cosine tapered illumination (6 dB edge taper).

D. Finite × Infinite Array Simulation

To investigate the effects of the array finiteness on the matching performance, the spectral method described in Sec. II-B is used. As an example, we consider a finite-by-infinite array with 25 elements along the finite direction. The active VSWR for all the elements is shown in Fig.13, for scanning to broadside and to 50° in both the E- and H-planes. Four elements (two on each edge) are not shown in the plot as they are assumed to be passively terminated. It can be seen that the curves oscillate significantly around the infinite array solution. This can cause mismatch of some elements, especially for scanning in the H-plane, resulting in narrower bandwidth and higher VSWR values, compared to the doubly periodic case. One way to mitigate these effects is to excite the array with a tapered illumination window. This approach is typically used in radar and Satcom applications to reduce the sidelobe levels at the cost of decreased aperture efficiency and total gain. As an example, a raised-cosine excitation with 6 dB edge taper is applied to the array in Fig. 14(b),(d) and (f). Smaller fluctuations can be observed with respect to the case of uniform illumination (Figs. 14(a),(c) and (e)).

IV. Design of the Feeding Structure

A possible implementation of the feeding structure is proposed in this section. The slot element of the array is fed with a microstrip line terminated by a shorting via. A microstrip-to-coaxial transition is designed to feed the elements with coaxial connectors, located underneath the backing reflector. The transmission coefficient (S_{12}) of the transition in isolation, shown in Fig. 14, is higher than -0.15 dB over the desired frequency band. Moreover, the transition is designed to implement a quarter wavelength section that transforms the input impedance at the slot (70 Ω) to 50 Ω at the connector. Due to the low impedance transformation ratio of the quarter-wave transformer, good impedance matching ($S_{11} < -20$ dB) is achieved by the transition within the wide bandwidth of investigation.

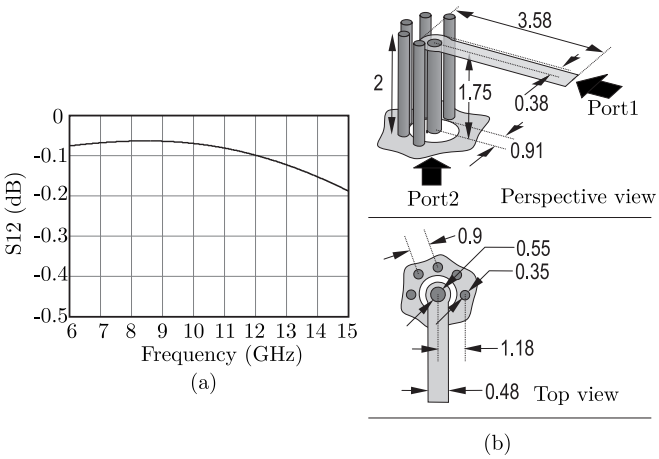

Fig. 14. (a) Transmission coefficient between ports 1 and 2 of the microstrip-to-coaxial transition; (b) geometrical parameters in mm.

A. Solution to Undesired PPW Modes

In Sec. II B, perfectly conducting walls were included between the slots to suppress the excitation of undesired PPW modes. We now clarify and demonstrate the effectiveness of this solution. When including the feed structure in the array unit cell in absence of metal walls, simulations exhibit strong resonances within the operative bandwidth, as reported in Fig. 15(a), for broadside and scanning in the main planes. Such resonances are caused by common-mode currents, excited on the integrated coaxial feed lines. This effect is described in Fig. 15(b), where two adjacent array elements are shown. The current impressed in one element of the array can flow to the vertical feed lines of the neighboring element generating unbalanced currents. The common-mode component of these currents excites PPW modes within the array substrate, resulting in the resonances observed in Fig. 15(a).

When continuous metallic walls are inserted between the slots as shown in Fig. 16(a), the propagation of the PPW modes is prevented, creating a choke for the common-mode current. The metal walls are parallel to the slot and are placed in the centers between adjacent slots. This configuration allows to minimize the influence on the slot impedance, since the currents flowing in the metal walls due to neighboring elements cancel out, giving a close-to-zero net current. This behavior is shown in Fig. 16(b). A practical implementation of the metal walls is obtained with metal plated vias in the

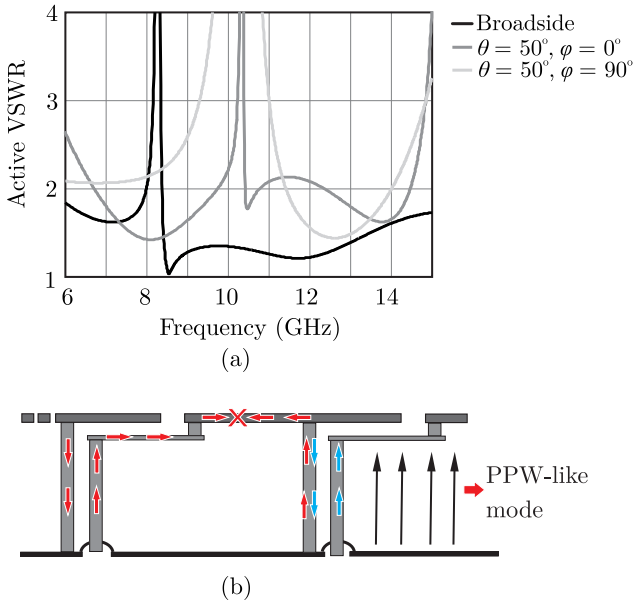

Fig. 15. (a) Common-mode resonances in the active VSWR of the array due to common-mode current excitation in the vertical feed lines; (b) schematic description of the common-mode current excitation.

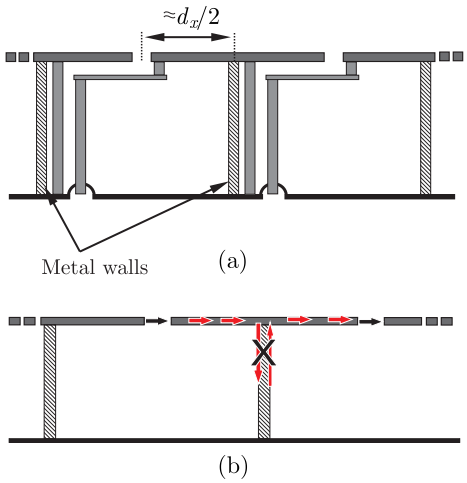

Fig. 16. (a) Introduction of the metallic walls to inhibit the propagation of the PPW modes; (b) current cancellation on the walls due to neighboring slots.

dielectric grid. The via holes, as depicted in Fig. 17, are spaced closely enough in terms of wavelength to emulate the properties of a continuous metal wall.

B. Array Performance

The simulations of the array including the details of the feed network have been performed with CST [23]. The active VSWR, including the metal wall as well the mini-SMP connector (see Fig. 17), is shown in Fig. 18. It can be observed that the presence of the walls eliminates the resonances highlighted in Fig. 15, resulting in a VSWR of less than 2 from 6.5 to 14.6 GHz.

Simulation assuming the finite conductivity of the metal have been performed to estimate the ohmic losses. The total

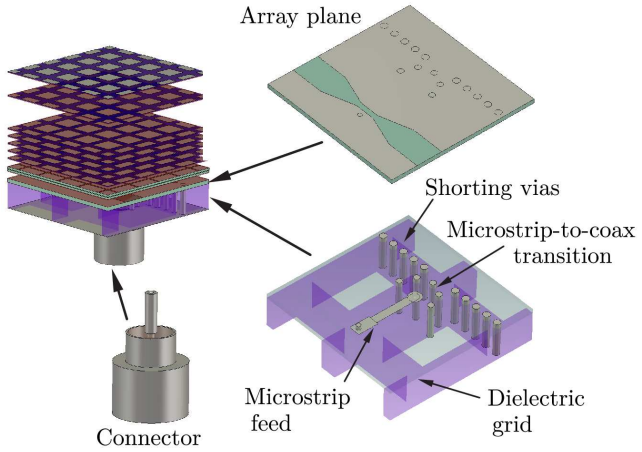

Fig. 17. A complete three-dimensional view of the unit cell array including the mini-SMP connector.

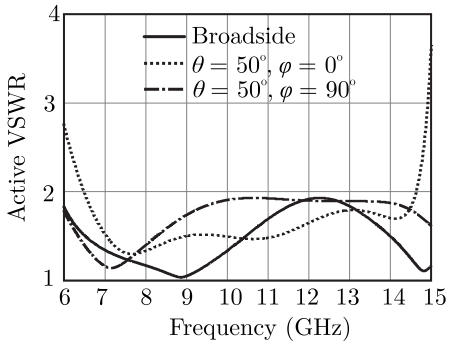

Fig. 18. Active VSWR of the array shown in Fig. 17.

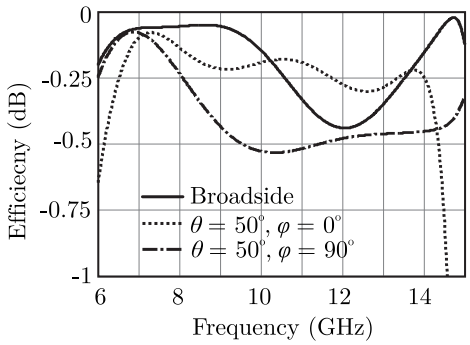

Fig. 19. The simulated efficiency of the array including ohmic and mismatch losses.

efficiency of the array, under infinite array approximation, is reported in Fig. 19. The curves show that the efficiency of the array is higher than 88% for all scanning angles. The main cause of losses is impedance mismatch, while negligible ohmic losses are predicted by the simulations. This distinctive property of the ADL was experimentally verified in [21].

V. Conclusions

We presented a novel concept for wideband wide-scanning phased array designs, based on connected arrays of slots loaded with ADL superstrates. The proposed structure has

two main advantages with respect to the existing solutions. Firstly, it is completely planar and realized with a single multi-layer PCB, with consequent reduction of the cost and the complexity of the array. Secondly, ADLs are used in place of real dielectric superstrates, to achieve much better efficiency in terms of surface-wave loss. The design of a wideband feed structure was also proposed, which does not require balanced-to-unbalanced (balun) transitions that limit the matching bandwidth.

For the design of the array loaded with ADL, including the adhesive layers, an analytical tool can be used which allows to estimate the performance of the array with minimal computational resources. This method was introduced for a doubly periodic array and then generalized to account for the finiteness in both transverse coordinates (x and y.)

The presented array has VSWR lower than 2 from 6.5 to 14.6 GHz for a single-polarized design. The array scans up to 50° in all azimuth planes with a radiation efficiency higher than 88%.

REFERENCES

[1] J. J. Lee, S. Livingston, and R. Koenig, "A low-profile wide-band (5:1) dual-pol array," *IEEE Antennas Wireless Propag. Lett.*, vol. 2, no. 1, pp. 46–49, 2003.

[2] J. J. Lee, S. Livingston, R. Koenig, D. Nagata, and L. L. Lai, "Compact light weight UHF arrays using long slot apertures," *IEEE Trans. Antennas Propag.*, vol. 54, no. 7, pp. 2009–2015, Jul. 2006.

[3] D. Cavallo, G. Gerini, R. Bolt, D. Deurloo, R. Grooters, A. Neto, G. Toso, and R. Midthassel, "Ku-band dual-polarized array of connected dipoles for satcom terminals: Theory and hardware validation," in *Proc. Eur. Conf. Antennas Propag.*, Gothenburg, Sweden, Apr. 2013, pp. 459–460.

[4] "The SKA website," Available: http://www.skatelescope.org/.

[5] D. H. Schaubert, A. O. Boryssenko, A. Van Ardenne, J. G. B. de Vaate, and C. Craeye, "The square kilometer array (SKA) antenna," in *Proc. IEEE Int. Symp. Phased Array Systems Tech.*, 14-17 Oct. 2003, pp. 351–358.

[6] A. W. Hotan et al., "The australian square kilometre array pathfinder: System architecture and specifications of the boolardy engineering test array," *Publ. Astron. Soc. Australia*, vol. 31, pp. e041, 2014.

[7] S. G. Hay and J. D. O'Sullivan, "Analysis of common-mode effects in a dual-polarized planar connected-array antenna," *Radio Sci.*, vol. 43, no. 10, Dec. 2008.

[8] L. Infante, A. De Luca, and M. Teglia, "Low-profile ultra-wide band antenna array element suitable for wide scan angle and modular subarray architecture," in *Proc. IEEE Int. Symp. Phased Array Systems Tech.*, 12-15 Oct. 2010, pp. 157–163.

[9] D. H. Schaubert, S. Kasturi, A. O. Boryssenko, and W. M. Elsallal, "Vivaldi antenna arrays for wide bandwidth and electronic scanning," in *Proc. Eur. Conf. Antennas Propag.*, Edinburgh, U.K., 11-16 Nov. 2007.

[10] Y.-S. Kim and K. S. Yngvesson, "Characterization of tapered slot antenna feeds and feed arrays," *IEEE Trans. Antennas Propag.*, vol. 38, no. 10, pp. 1559–1564, Oct. 1990.

[11] R. C. Hansen, "Linear connected arrays," *IEEE Antennas Wireless Propag. Lett.*, vol. 3, no. 1, pp. 154–156, Dec. 2004.

[12] D. Cavallo, A. Neto, G. Gerini, A. Micco, and V. Galdi, "A 3- to 5-GHz wideband array of connected dipoles with low cross polarization and wide-scan capability," *IEEE Trans. Antennas Propag.*, vol. 61, no. 3, pp. 1148–1154, Mar. 2013.

[13] J. P. Doane, K. Sertel, and J. L. Volakis, "A wideband, wide scanning tightly coupled dipole array with integrated balun (TCDA-IB)," *IEEE Trans. Antennas Propag.*, vol. 61, no. 9, pp. 4538–4548, Sep. 2013.

[14] S. S. Holland, D. H. Schaubert, and M. N. Vouvakis, "A 7-21 GHz dual-polarized planar ultrawideband modular antenna (PUMA) array," *IEEE Trans. Antennas Propag.*, vol. 60, no. 10, pp. 4589–4600, Oct. 2012.

[15] D. Cavallo, A. Neto, and G. Gerini, "Analytical description and design of printed dipole arrays for wideband wide-scan applications," *IEEE Trans. Antennas Propag.*, vol. 60, no. 12, pp. 6027–6031, Dec. 2012.

[16] D. Cavallo, A. Neto, and G. Gerini, "Common-mode resonances in ultra wide band connected arrays of dipoles: Measurements from the demonstrator and exit strategy," in *Proc. Int. Conf. Electromagnetics Advanced Applications*, Turin, Italy, 14-18 Sep. 2009, pp. 435–438.

[17] A. Neto, D. Cavallo, G. Gerini, and G. Toso, "Scanning performances of wideband connected arrays in the presence of a backing reflector," *IEEE Trans. Antennas Propag.*, vol. 57, no. 10, pp. 3092–3102, Oct. 2009.

[18] D. Cavallo, A. Neto, and G. Gerini, "A 10.5-14.5 GHz wide-scanning connected array of dipoles with common-mode rejection loops to ensure polarization purity," in *Proc. IEEE Int. Symp. Antennas Propag. Soc.*, Toronto, ON, Canada, 11-17 Jul. 2010.

[19] D. Cavallo, W. H. Syed, and A. Neto, "Closed-form analysis of artificial dielectric layers—Part I: Properties of a single layer under plane-wave incidence," *IEEE Trans. Antennas Propag.*, vol. 62, no. 12, pp. 6256–6264, Dec. 2014.

[20] D. Cavallo, W. H. Syed, and A. Neto, "Closed-form analysis of artificial dielectric layers—Part II: Extension to multiple layers and arbitrary illumination," *IEEE Trans. Antennas Propag.*, vol. 62, no. 12, pp. 6265–6273, Dec. 2014.

[21] W. H. Syed and A. Neto, "Front-to-back ratio enhancement of planar printed antennas by means of artificial dielectric layers," *IEEE Trans. Antennas Propag.*, vol. 61, no. 11, pp. 5408–5416, Nov. 2013.

[22] A. Neto and J. J. Lee, "Ultrawide-band properties of long slot arrays," *IEEE Trans. Antennas Propag.*, vol. 54, no. 2, pp. 534–543, Feb. 2006.

[23] "CST Microwave Studio 2012," Available: http://www.cst.com.

[24] A. Neto, D. Cavallo, and G. Gerini, "Edge-born waves in connected arrays: A finite×infinite analytical representation," *IEEE Trans. Antennas Propag.*, vol. 58, no. 10, pp. 3646–3657, Oct. 2011.

[25] D. Cavallo and A. Neto, "A connected array of slots supporting broadband leaky waves," *IEEE Trans. Antennas Propag.*, vol. 61, no. 4, pp. 1986–1994, Apr. 2013.

[26] C. Menzel, C. Rockstuhl, T. Paul, F. Lederer, and T. Pertsch, "Retrieving effective parameters for metamaterials at oblique incidence," *Phys. Rev. B*, vol. 77, no. 19, pp. 195328, May 2008.

[27] S. Maci, G. Minatti, M. Casaletti, and M. Bosiljevac, "Metasurfing: Addressing waves on impenetrable metasurfaces," *IEEE Antennas Wireless Propag. Lett.*, vol. 10, pp. 1499–1502, 2011.

[28] D. Cavallo, A. Neto, and G. Gerini, "Greens function based equivalent circuits for connected arrays in transmission and in reception," *IEEE Trans. Antennas Propag.*, vol. 59, no. 5, pp. 1535–1545, May 2011.

Waqas H. Syed (S'11) received the B.Sc. degree with distinction in telecommunication engineering from the CIIT, Islamabad, Pakistan, in 2007, his M.Sc. degree from RWTH Aachen University, Aachen, Germany, in 2010, and his Ph.D. degree (*cum laude*) in electromagnetics from Delft University of Technology (TUDelft), Delft, Netherlands, in 2015.

Currently, he is working as Post-Doctoral researcher in the Terahertz Sensing Group at TUDelft. His research interests include artificial dielectrics and the design of integrated antennas and arrays.

Dr. Syed was recipient of the Special Mention for Excellent Presentation at the European Conference on Antennas and Propagation (EuCAP) in 2015.

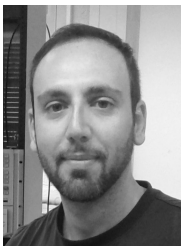

Daniele Cavallo (S'09−M'11) received the M.Sc. degree (*summa cum laude*) in telecommunication engineering from the University of Sannio, Benevento, Italy, in 2007, and his Ph.D. degree (*cum laude*) in electromagnetics from Eindhoven University of Technology (TU/e), Eindhoven, Netherlands, in 2011.

From 2007 to 2011, he was with the Antenna Group at the Netherlands Organization for Applied Scientific Research (TNO), The Hague, Netherlands. In the years 2012-2015, he was Post-Doctoral researcher in the Microelectronics department of Delft University of Technology (TUDelft), Delft, Netherlands. During 2015, he spent two months as a visiting researcher at Chalmers University of Technology in Gothenburg, Sweden. From September 2015, he is assistant professor in the Terahertz Sensing Group at TUDelft. He is the author or coauthor of more than 70 papers published in peer-reviewed international journals and conference proceedings. His research interests include analytical and numerical methods for antenna characterization, the design of antenna arrays and high-frequency on-chip antennas.

Dr. Cavallo was first author of the paper awarded with the best innovative paper prize at the 30th ESA Antenna Workshop in 2008 and nominee for the best doctoral project in the TU/e Academic Annual Awards 2012. He has been awarded a three-year personal grant from the Netherlands Organization for Scientific Research (NWO VENI, 250 keuro), for developing "Efficient On-Chip Antennas for Terahertz Applications". He is a member of the European Association on Antennas and Propagation (EurAAP).

Andrea Neto (M'00−SM'10) received the Laurea degree (*summa cum laude*) in electronic engineering from the University of Florence, Florence, Italy, in 1994 and the Ph.D. degree in electromagnetics from the University of Siena, Siena, Italy, in 2000.

Part of his Ph.D. degree was developed at the European Space Agency Research and Technology Center, Noordwijk, The Netherlands, where he worked for the antenna section for over two years. In the years 2000−2001, he was a Post-Doctoral Researcher at the California Institute of Technology, Pasadena, CA, USA, working for the Sub-Millimeter-Wave Advanced Technology Group. From 2002 to January 2010, he was a Senior Antenna Scientist at TNO Defence, Security, and Safety, The Hague, The Netherlands. In February 2010, he was appointed Full Professor of Applied Electromagnetism in the Electrical Engineering, Mathematics and Computer Science Department, Technical University of Delft, Delft, The Netherlands, where he formed and leads the THz Sensing Group. His research interests are in the analysis and design of antennas, with emphasis on arrays, dielectric lens antennas, wideband antennas, EBG structures, and THz antennas.

Prof. Neto was corecipient of the H. A. Wheeler award for the best applications paper of the year 2008 in the IEEE TRANSACTIONS ON ANTENNAS AND PROPAGATION. He was corecipient of the best innovative paper prize at the 30th ESA Antenna Workshop in 2008. He was corecipient of the best antenna theory paper prize at the European Conference on Antennas and Propagation (EuCAP) in 2010. He served as an Associate Editor of the IEEE TRANSACTIONS ON ANTENNAS AND PROPAGATION (2008−2013) and IEEE ANTENNAS AND WIRELESS PROPAGATION LETTERS (20052013). He is member of the Technical Board of the European School of Antennas and organizer of the course on Antenna Imaging Techniques. He is a member of the steering committee of the network of excellence NEWFOCUS, dedicated to focusing techniques in mm and sub-millimeter-wave regimes. In 2011 he was awarded the European Research Council Starting Grant to perform research on Advanced Antenna Architectures for THz Sensing Systems. He was the Awards and Grants Chair for EUCAP 2014.